

**Development of silicon electrode enhanced by carbon nanotube and gold nanoparticle composites on silicon neural probe fabricated with complementary metal-oxide-semiconductor process**

Songsong Zhang, Wei Mong Tsang, Merugu Srinivas, Tao Sun, Navab Singh, Dim-Lee Kwong, and Chengkuo Lee

Citation: [Applied Physics Letters](#) **104**, 193105 (2014); doi: 10.1063/1.4875961

View online: <http://dx.doi.org/10.1063/1.4875961>

View Table of Contents: <http://scitation.aip.org/content/aip/journal/apl/104/19?ver=pdfcov>

Published by the [AIP Publishing](#)

---

**Articles you may be interested in**

[Paper-based ultracapacitors with carbon nanotubes-graphene composites](#)

J. Appl. Phys. **115**, 164301 (2014); 10.1063/1.4871290

[Effect of nano-filler on the performance of multiwalled carbon nanotubes based electrochemical double layer capacitors](#)

J. Renewable Sustainable Energy **6**, 013108 (2014); 10.1063/1.4861889

[Photoresponse from noble metal nanoparticles-multi walled carbon nanotube composites](#)

Appl. Phys. Lett. **101**, 241113 (2012); 10.1063/1.4771125

[Determination and enhancement of the capacitance contributions in carbon nanotube based electrode systems](#)

Appl. Phys. Lett. **95**, 183108 (2009); 10.1063/1.3258353

[Supercapacitor electrodes from multiwalled carbon nanotubes](#)

Appl. Phys. Lett. **77**, 2421 (2000); 10.1063/1.1290146

---



## Development of silicon electrode enhanced by carbon nanotube and gold nanoparticle composites on silicon neural probe fabricated with complementary metal-oxide-semiconductor process

Songsong Zhang,<sup>1,2,3</sup> Wei Mong Tsang,<sup>2</sup> Merugu Srinivas,<sup>2</sup> Tao Sun,<sup>2</sup> Navab Singh,<sup>2</sup> Dim-Lee Kwong,<sup>2</sup> and Chengkuo Lee<sup>1,3,a)</sup>

<sup>1</sup>Department of Electrical and Computer Engineering, National University of Singapore,

4 Engineering Drive 3, Singapore 117576

<sup>2</sup>Institute of Microelectronics (IME), Agency for Science, Technology and Research (A-STAR), Singapore 117685

<sup>3</sup>Singapore Institute for Neurotechnology (SiNAPSE), National University of Singapore, 28 Medical Drive, #05-COR, Singapore 117456

(Received 24 March 2014; accepted 29 April 2014; published online 13 May 2014)

We present the fabrication of highly P-doped single crystal silicon electrodes on a silicon probe through complementary metal-oxide-semiconductor (CMOS)-compatible processes. The electrode with diameter of 50  $\mu\text{m}$  and a separation of 200  $\mu\text{m}$  is designed for recording/stimulating purposes. Electrochemical impedance spectroscopy indicates that the interfacial impedance of silicon electrodes at 1 KHz is  $2.5 \pm 0.4 \text{ M}\Omega$ , which is equivalent to the result reported from the gold (Au) electrode. To further enhance the charge storage capacity, composites of multi-wall carbon nanotubes (MWCNTs) and Au nanoparticles are electroplated onto the highly P-doped silicon electrode after surface roughness treatments. With optimized electroplating processes, MWCNTs and Au nanoparticles are selectively coated onto the electrode site with only a minimum enlargement in physical diameter of electrode ( $<10\%$ ). However, the typical impedance is reduced to  $21 \pm 3 \text{ k}\Omega$ . Such improvement can be explained by a boost in double-layer capacitance ( $C_{dl}$ ) and the reduction in faradic resistances. The measurement of cyclic voltammetry (CV) shows that the cathodal charge storage capacity is up to  $35 \text{ mC cm}^{-2}$ , which proves the superior performance of composite coatings on silicon electrodes and validates the functionality of reported CMOS-compatible silicon probe.

© 2014 AIP Publishing LLC. [<http://dx.doi.org/10.1063/1.4875961>]

Establishing electrical communications between human body and outside world helps us to understand the brain function and pathway of nervous systems. Sharpened metal wire electrodes were used to record the extracellular potential or electrically depolarize membranes of excitable cells.<sup>1</sup> In past few decades, significant progresses in Microelectromechanical systems (MEMS) technology facilitate the migration of neural prosthetic device (NPD) from the bulky metal wire to the MEMS based micro-scaled silicon probe. The succession of Utah and Michigan probes validates the chronic stability and mechanical property of the silicon material for the application as NPDs.<sup>2,3</sup> In order to record a good quality neural signal from background noises, the silicon probe should be placed in a close proximity to neurons (in the range of 50  $\mu\text{m}$ ). In general, a high electrode density silicon probe with of an extracellular potential recording resolution better than 50  $\mu\text{m}$  is desirable.<sup>4</sup> In addition, a clearer understanding of brain functions and neuron mappings in system level also requires the simultaneous recording and stimulation from many sites and spatial locations. Resultant two-dimensional (2-D)<sup>4</sup> and even three-dimensional (3-D)<sup>5-7</sup> microelectrode arrays (MEAs) with numerous signal pathways demand large amounts of complicated data processing, hence, the on-chip integration of both MEMS and CMOS technologies is indispensable for

sophisticated system level neural signal analyses. Tremendous research efforts have been dedicated into the development of monolithically fabricated MEAs. By far, the post-fabrication method of recording/stimulating electrodes after completion of CMOS circuitry is usually the solution to realize the direct on-chip integration.<sup>4</sup>

As another inevitable consequence of high density MEAs, the dimension of each electrode has to be dramatically reduced to minimize the probe geometry so that avoid large tissue damages during the insertion. However, the shrinkage of the geometric surface area (GSA) will increase the electrode impedance, which introduces higher Johnson noise during the recording and degrades the efficiency of charge transfer during the stimulation.<sup>8</sup> Noble metals such as gold (Au) and platinum (Pt) fail to deliver enough charge within a limited GSA. In the past decade, the activated iridium oxide film (AIROF) has been widely implemented as extra coatings on metal electrodes.<sup>3,4</sup> AIROF generally provides a higher charge storage capacity (CSC)<sup>9</sup> and also suits the requirement of most post-fabrication processes on silicon substrate. However, the delamination of AIROF particles under high stimulation charge has been reported due to its intrinsic faradaic charge transferring nature.<sup>10</sup> Recently, the emerging material like carbon nanotubes (CNTs) has drawn the great interest by researchers.<sup>11</sup> Besides the excellent mechanical property and the superior CSC, randomly oriented multi-wall CNTs (MWCNTs) have been reported with the capability of forming intimate contacts with cells and

<sup>a)</sup> Author to whom correspondence should be addressed. E-mail: [elec@nus.edu.sg](mailto:elec@nus.edu.sg)

facilitate the neuron growth.<sup>8,12</sup> Moreover, it has been widely incorporated with other conductive materials to establish better electrode-neuron interfaces.<sup>13–15</sup> Benefiting by high conductivity, minimal toxicity, and fabrication simplicity, Au nanoparticle is another promising conductive material introduced in NPD designs.<sup>15</sup> In addition, remarkable performance improvements after coating the incorporative composite consisting of both CNTs and Au nanoparticles have been recently reported, but the application of this composite material is mostly limited with noble metal electrodes on only polymer substrates.<sup>17,18</sup>

In this paper, we demonstrate the fabrication of the prototype of silicon neural probe with 100 nm thick highly boron-doped single crystal silicon layer as the electrode. Consequently, both silicon electrodes and standard aluminum (Al) interconnections simplify the monolithic fabrication process. As a result, the complicated post-fabrication of electrodes using noble metals can be avoided. The optical image of the device and the schematic drawing are shown in Figs. 1(a) and 1(b), respectively. The exploded view of the probe tip is given in the inset of Fig. 1(b) to provide a better understanding of the monolithic fabrication process. Additionally, the highly doped silicon electrode may also enhance the signal to noise ratio<sup>16</sup> and reduce leakage currents.<sup>11</sup> To further improve CSC and device bio-compatibility, we demonstrate the electroplating of MWCNTs and Au nanoparticle composites onto silicon surface electrodes with a precise control. In the following content, we will introduce the optimized electroplating process of MWCNTs and Au nanoparticles on highly doped silicon electrodes. The resultant improvement in charge injections and effects on lowering the interfacial impedance will also be discussed in detail.

Fabrications are starting with 8 in. (100) plane silicon on insulator (SOI) wafers (SOITEC, nominal resistivity: 8.5–11.5  $\Omega$  cm) with 117 nm device layer on top of a 145 nm buried thermal oxide layer (BOX). The 1st boron (p-type) global implantation is performed with a dosage of  $4 \times 10^{15}$  ion/cm<sup>2</sup>. The rapid thermal annealing (1050 °C, 30 s) is then

carried for the dopant activation. Based on the measurement from the test structure (a rectangular silicon block with dimension of  $330 \mu\text{m} \times 100 \mu\text{m} \times 110 \text{nm}$  and resistance of 400  $\Omega$ ), the estimated impurity carrier concentration is around  $1 \times 10^{20} \text{cm}^{-3}$ . After the standard photolithography process, the electrode with diameter of  $50 \mu\text{m}$  is defined on the doped silicon layer with the BOX layer as the etching stopper. Sequentially, 400 nm SiO<sub>2</sub> passivation layer is coated on top using Plasma-Enhanced Chemical Vapor Deposition (PECVD). Numbers of via are then patterned and etched (as indicated in the inset of Fig. 1(b)). After the 2nd boron doping (dosage of  $4 \times 10^{15}$  ion/cm<sup>2</sup>) on only via regions and the sequential Al metallization, the electrical linkage between top Al layer and bottom highly doped silicon layers is formed through via openings on PECVD oxide layer. 1  $\mu\text{m}$  PECVD low stress silicon nitride (SiN<sub>x</sub>) cladding layer is coated to encapsulate aluminum traces away from tissues. Both bonding pads and electrode sites opening are defined through Reactive Ion Etching (RIE) processes. The shape of the probe is defined through the Deep Reactive Ion Etching (DRIE) down to  $60 \mu\text{m}$  from the front side of wafers. The final backside grinding releases the probe with the thickness of  $50 \mu\text{m}$  and various lengths (up to 7 mm). The detailed electrode arrangement on the probe tip and the equivalent schematic for the cross section of a released probe are given in the inset of Figs. 1(a) and 1(c), respectively. Serving the purpose of prototype design, the probe with single shaft is made, but the same fabrication technique can also be extended to array designs.

The electrode surface treatment is performed before electroplating of MWCNTs and Au nanoparticles. This step is also found to be compulsory to ensure a successful electroplating process on silicon electrodes. The treatment process is completed through xenon difluoride (XeF<sub>2</sub>) vapor etching ( $\sim 2\text{s}$ ) in the reticle level. As a result, the original smooth silicon surface turns to porous, thus, creating enough roughness on silicon electrodes. Optical images of the doped silicon electrode before and after the surface treatment are displayed in Figs. 2(a) and 2(b). The obvious color change is caused by the partial exposure of the beneath BOX layer. In addition, the surface morphology after the treatment is also confirmed by the image taken from scanning electron microscope (SEM) and shows in Fig. 2(f). In the next step, the CNT and Au nanoparticle composite coating is applied from an aqueous solution (2 mg/ml) consisting of MWCNTs (Cheap Tubes Inc., length  $\sim 0.5\text{--}2 \mu\text{m}$ , outer diameter  $< 8 \text{nm}$ ) mixed into an Au electrolyte bath (TSG-250, Transene) with applied sine wave pulses (amplitude 1.5 Vpp, 0.75 V DC offset, 50% duty cycle, 60 s). The cathode is connected to the silicon electrode, and Au wire (diameter  $\sim 1 \text{mm}$ ) is connected to the anode.<sup>16</sup> With the assistance of Au nanoparticles (Au ions) in the solution, both Au nanoparticles and Au encapsulated MWCNTs are deposited onto the surface of the electrode during the cathodic cycle. The optical image of a porous silicon electrode after coating is provided in Fig. 2(c). MWCNTs and Au nanoparticle composites are electroplated only onto the electrically conductive region (highly doped silicon electrode) without contaminations of rest areas. In addition, the enlargement of electrode GSA is well controlled to be less than 10% ( $< 55 \mu\text{m}$  in diameter) of its

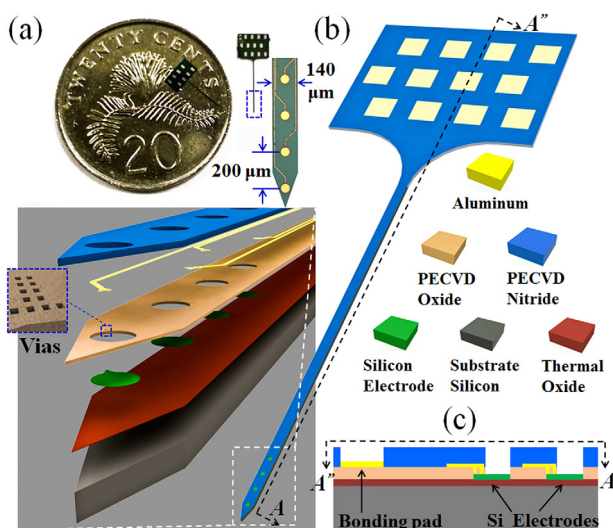


FIG. 1. (a) The optical image of silicon probes and an inset of the zoom-in image on the probe tip. (b) The schematic drawing of reported silicon probe with an exploded view of the probe tip. (c) An illustration on the cross-section of a released probe.

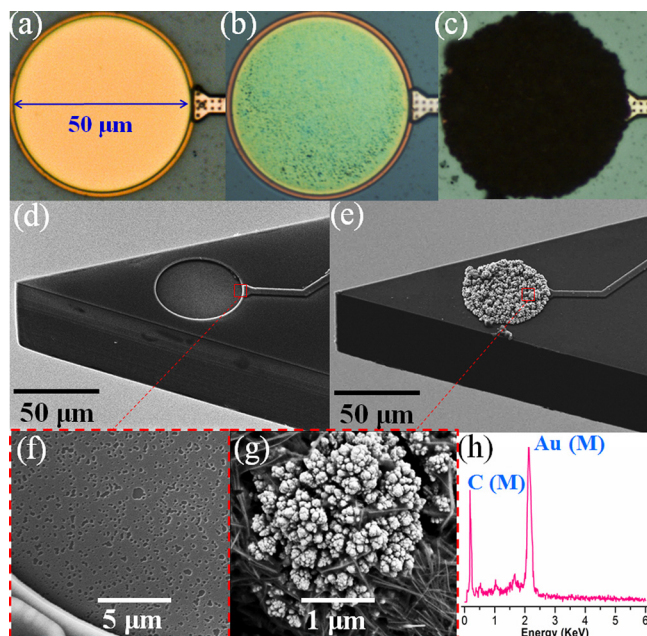


FIG. 2. Optical images on the silicon electrode (a) before the surface treatment, (b) after the surface treatment, and (c) after depositions of MWCNTs plus Au nanoparticles; SEM pictures on the probe tip (d) before and (e) after depositions of MWCNTs plus Au nanoparticles; (f) SEM picture on surface morphology after the surface treatment; (g) SEM picture on Au nanoparticles and fibrous MWCNT; (h) A plot of EDX results for the region shown in (g).

original size. SEM photos in Figs. 2(d) and 2(e) indicate the difference on the probe before and after electroplating processes. The composite coating on Si electrode survives after 10 s ultrasonic shaking conducted in ultrasonic cleaner (Branson B3510, 40 kHz, Max input power of 130 W). However, qualitative characterizations on the adhesion between composite coatings and silicon electrodes have to be further conducted through *in vivo* experiment in future. Fig. 2(g) shows the surface morphology of the Au nanoparticles, which is described as white globular dots with MWCNTs randomly orientated in fibrous shapes. Energy-dispersive X-ray (EDX) analysis (Fig. 2(h)) confirms the presence of both Au and CNTs on coated electrodes. It is also worth noting that the original silicon electrode (without surface treatment) fails to be electroplated even with a higher biasing voltage during electroplating. Low surface roughnesses and a thin layer of surface native oxide are reasonable explanations for such failures.

Electrochemical impedance spectroscopy (EIS) is conducted to first verify the change of interfacial impedances. Phosphate buffered saline (PBS, Biowest, pH 7.4, conductivity  $\times 1$ ) is used as the *in vitro* medium. The sine wave with amplitude of 50 mV and frequency spans from 100 KHz to 0.7 Hz are applied. Three-electrode technique is used in the experiment with the silver/silver chloride (Ag/AgCl) electrode and a Pt wire as reference and counter electrode, respectively. The output impedance is recorded *in vitro* with an impedance analyzer (Autolab PGSTAT100N voltage potentiostat/galvanostat, Metrohm), and results are plotted in Fig. 3. Impedances of smooth and porous surface silicon electrode at 1 KHz are recorded as  $2.5 \pm 0.4$  M $\Omega$  and  $0.9 \pm 0.2$  M $\Omega$ , respectively. The reduced impedance of the porous surface over flat surface electrode is due to the increment of electrochemical surface area (ESA).<sup>7</sup> Such impedance

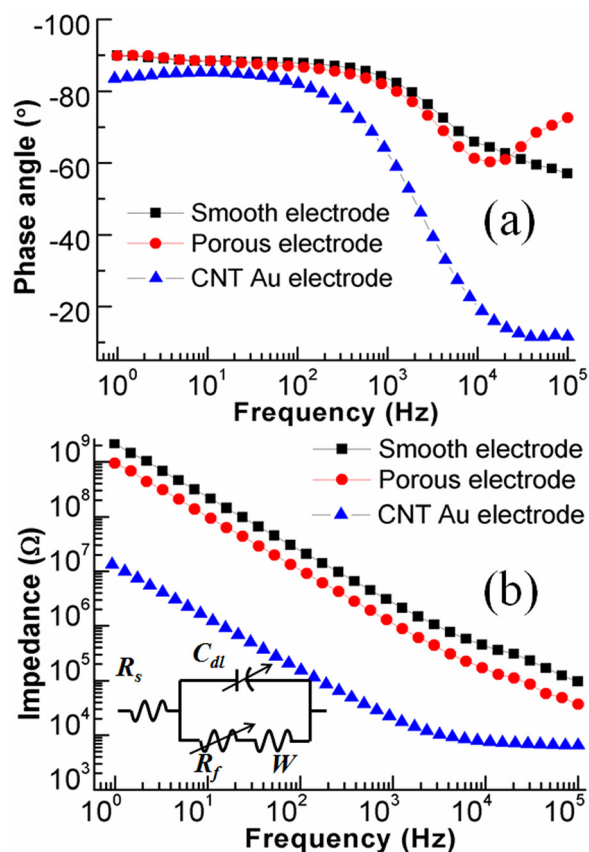


FIG. 3. Results from EIS for (a) the plot of phase angle and (b) the plot of interfacial impedances for smooth, porous, and MWCNTs & Au nanoparticles coated silicon electrodes. The inset shows Randles equivalent circuit.

value can be categorized in the same level as the result obtained from the equivalent GSA of Au electrode. After deposition of CNT and Au composites, the impedance drops by two orders ( $21 \pm 3$  K $\Omega$ ). The drastic decrease of the interfacial impedance is credited by the high porosity of surface coatings contributed from both CNTs and Au nanoparticles. Such highly porous electrode surface is essential for the large ESA and the resultant huge amount of charge accumulations between electrode-electrolyte interfaces. It has been reported that the specific surface area of plasma treated MWCNTs is up to  $400 \text{ m}^2 \text{ g}^{-1}$ .<sup>19</sup> As a result, the larger amount of charge can be accumulated on CNTs external surfaces than the amount of charge on the traditional planar electrode. In addition, the larger ESA also provides higher electrolyte accessibility over the planar surface electrode. Moreover, it has been proposed that ions can be squeezed into the inner cavity of nanotubes, if the tube has an opening tip. With a small inner diameter of CNTs ( $< 8$  nm in our case), the distance ( $d$ ) between tube internal surface and the maximum charge density of electrolyte ions would be deduced. Thus, according to  $C = \epsilon A/d$  (where  $C$  is capacitance,  $\epsilon$  is permittivity of the electrolyte, and  $A$  is the ESA between electrode and electrolyte), a further increment in total capacitance. On the other hand, the electrical conductivity of macro-scale composites made from Au is higher than other CNT composites. With the Layer-by-layer assembly method, an even better CSC of Au particles in nano-scale than that of pure CNTs has been observed.<sup>15</sup> Thus, the combination of both CNT and Au nanoparticle will take full advantages of the superior mechanical

property of CNT as well as the high CSC from both CNTs and Au nanoparticles. To further interpret the improvement of CSC quantitatively, the Randles equivalent circuit (illustrated in the inset of Fig. 3(b)) is introduced, and changes in double-layer capacitance are analyzed as below.

In a simple case, Randles circuit consists of a double-layer capacitor ( $C_{dl}$ ) in parallel with the series combination of a charge-transfer resistance or Faradaic resistance ( $R_f$ ) and Warburg impedance ( $W$ ). When a potential is applied through the measurement system, another series resistance ( $R_s$ ), which includes the solution resistance (between the working and reference electrodes) plus the electrical resistance of testing electrodes, is added into the circuit as well. The Warburg impedance is generally negligible at high frequencies. The time interval is too short to be sufficient for the ion diffusion reacted on the electrode surface.<sup>20</sup> Thus, the expression of total impedance can be simplified as

$$Z(\omega) = R_s + \frac{R_f}{1 + j\omega R_f C_{dl}} = Z'(\omega) + Z''(\omega), \quad (1)$$

where  $\omega$  is the angular frequency,  $Z'$  is the real part of total impedance, and  $Z''$  is the imaginary part of total impedance. The series resistance ( $R_s$ ) approximates to the value of total impedance ( $Z$ ) as the frequency ( $f$ ) tends to be very high ( $f \rightarrow \infty$ ). Under such assumption,  $R_f$  and  $C_{dl}$  of at each frequency can be determined by<sup>19</sup>

$$R_f(\omega) = \frac{Z''^2 + (Z' - R_s)^2}{Z' - R_s}, \quad (2)$$

$$C_{dl}(\omega) = -\frac{Z''}{\omega[(Z' - R_s)^2 + Z''^2]}, \quad (3)$$

assuming the working electrode is placed within 5 mm radius from the reference electrode and the conductivity of PBS is specified as 14 000–17 800  $\mu\Omega^{-1}/\text{cm}$ . Thus, series resistances of both smooth and porous silicon electrodes can be assumed to equal to their electrical resistances due to the negligibly small solution resistances (in the range of few tens of Ohms). After the measurement of testing structures, the electrical resistance before coating of composite is around 1–1.5 k $\Omega$ . After deposition of CNTs and Au composites, the estimated series resistance is around 6.5 k $\Omega$  based on the observation from EIS plotted in Fig. 3(b). Angular information can be obtained from the plot of phase changes in Fig. 3(a). As results, information on double-layer capacitance and faradaic resistance changes at 1 kHz before and after composite depositions is summarized in Table I according to Eqs. (2) and (3). Based on information provided in Table I, the significant improvement in interfacial impedances is contributed from

TABLE I. Parameters extracted from the Randles equivalent circuit based on Si electrodes with different cases of surface conditions.

P-doped silicon electrodes	$R_s$ (k $\Omega$ )	$R_f$ (M $\Omega$ )	$C_{dl}$ ( $\mu\text{F}$ )
Before treatment	~1	~62	~0.7
After treatment	~1.5	~4	~1.1
After coating	~6.5	~0.14	~46.7

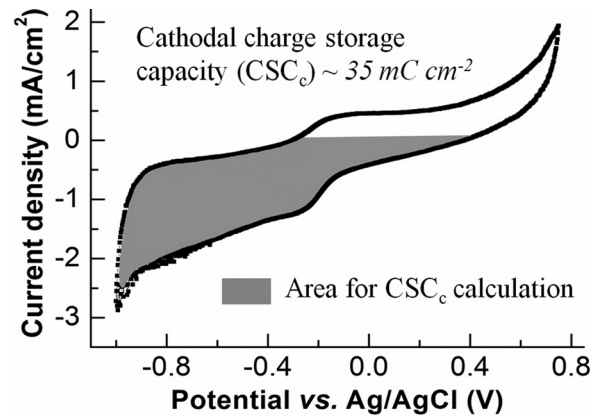


FIG. 4. Cyclic voltammetry plot of the silicon electrode after coating with MWCNTs plus Au nanoparticles.

the combination of an increment of double layer capacitances ( $C_{dl}$ ) and a decrement in faradaic resistances ( $R_f$ ). This interpretation also stands for the improvement of silicon electrode after surface treatments over the smooth surface counterpart.

Manintaining the same testing setup, the CSC of electrodes after composite coating is evaluated by the cyclic voltammetry (CV) under a sweep rate of 50 mV s<sup>-1</sup>. The resulting CV curve is plotted in Fig. 4, and the electrolysis window is very similar to the literature.<sup>9</sup> According to our tests, oxygen and hydrogen evolve at +0.75 and -1 V (vs. Ag/AgCl), respectively. There are small peaks at about -0.25 V, which is most likely contributed by the reduction of absorbed oxygen.<sup>9</sup> In addition, the relatively featureless CV window suggests that silicon electrodes after coating composites exhibit charging and discharging behaviors with the presence of only double-layer capacitance instead of faradic reactions. This pure capacitive charge transferring mechanism implies a safer working range without introducing irreversible electrochemical reactions.<sup>7</sup> The cathodal charge storage capacity (CSC<sub>c</sub>) is calculated from the time integral of the cathodic current in CV over a potential range just within water electrolysis window. The CSC<sub>c</sub> of the highly doped silicon electrode after MWCNTs and Au nanoparticles coating is around 35 mC cm<sup>-2</sup>, which is higher than the CSC<sub>c</sub> reported from AIROF<sup>7</sup> and in the equivalent range to some results reported on other conductive material composites (e.g., Poly(3,4-ethylenedioxythiophene) (PEDOT)/MWCNT composites).<sup>13</sup>

In conclusion, we demonstrate the fabrication of highly P-doped single crystal silicon electrodes on the silicon probe through CMOS-compatible processes. *In vitro* EIS results prove the functionality of our prototype device. After surface treatment and nano-composite coating processes, a superior charge injection capability suggests that our reported Si probe is potentially competent for both neural recording/stimulation purposes. The resultant performance of our device is competitive to those silicon neural prosthetic devices prepared by complicated post-fabrication techniques using noble metals.

This work was supported by grants from the National Research Foundation (NRF) CRP project 'Self-Powered Body Sensor Network for Disease Management and Prevention

Oriented Healthcare' (R-263-000-A27-281) and National Research Foundation (NRF) CRP project 'Peripheral Nerve Prostheses: A Paradigm Shift in Restoring Dexterous Limb Function' (R-719-000-001-281).

- <sup>1</sup>D. A. Robinson, *Proc. IEEE* **56**, 1065 (1968).
- <sup>2</sup>P. J. Rousche and R. A. Normann, *J. Neurosci. Methods* **82**, 1 (1998).
- <sup>3</sup>K. D. Wise, A. M. Sodagar, Y. Yao, M. N. Gulari, G. E. Perlin, and K. Najafi, *Proc. IEEE* **96**(7), 1184 (2008).
- <sup>4</sup>K. Seidl, S. Herwik, T. Torfs, H. P. Neves, O. Paul, and P. Ruther, *IEEE J. Microelectromech. Syst.* **20**(6), 1439 (2011).
- <sup>5</sup>S. Spieth, O. Brett, K. Seidl, A. A. Aarts, M. A. Erisimis, S. Herwik, F. Trenkle, S. Tatzner, J. Auber, M. Daub *et al.*, *J. Micromech. Microeng.* **21**, 125001 (2011).
- <sup>6</sup>K. Kwon, B. Sirowatka, A. Weber, and W. Li, *IEEE Trans. Biomed. Circuits Syst.* **7**(5), 593 (2013).
- <sup>7</sup>Y.-T. Lee, C.-W. Lin, C.-M. Lin, S.-R. Yeh, Y.-C. Chang, and W. Fang, *J. Micromech. Microeng.* **20**, 025014 (2010).
- <sup>8</sup>A. O. Fung, C. Tsiokos, O. Paydar, L. H. Chen, S. Jin, Y. Wang, and J. W. Judy, *Nano Lett.* **10**, 4321 (2010).
- <sup>9</sup>S. F. Cogan, *Annu. Rev. Biomed. Eng.* **10**, 275 (2008).
- <sup>10</sup>S. F. Cogan, A. A. Guzelian, W. F. Agnew, T. G. H. Yuen, and D. B. McCreery, *J. Neurosci. Methods* **137**, 141 (2004).
- <sup>11</sup>K. Wang, H. A. Fishman, H. Dai, and J. S. Harris, *Nano Lett.* **6**(9), 2043 (2006).
- <sup>12</sup>G. Cellot, E. Cilla, S. Cipollone, V. Rancic, A. Sucapane, S. Giordan, L. Gambazzi, H. Markram, M. Grandolfo, D. Scaini *et al.*, *Nat. Nanotechnol.* **4**, 126 (2009).
- <sup>13</sup>H. H. Zhou, X. Cheng, L. Rao, T. Li, and Y. Y. Duan, *Acta Biomater.* **9**, 6439 (2013).
- <sup>14</sup>S. Chen, W. Pei, Q. Gui, R. Tang, Y. Chen, S. Zhao, H. Wang, and H. Chen, *Sens. Actuators, A* **193**, 141 (2013).
- <sup>15</sup>H. Zhang, J. Shih, J. Zhu, and N. A. Kotov, *Nano Lett.* **12**, 3391 (2012).
- <sup>16</sup>R. Saha, N. Jackson, C. Patel, and J. Muthuswamy, *IEEE Trans. Neural Syst. Rehabil. Eng.* **18**(5), 489 (2010).
- <sup>17</sup>E. W. Keefer, B. R. Botterman, M. I. Romero, A. F. Rossi, and G. W. Gross, *Nat. Nanotechnol.* **3**, 434 (2008).
- <sup>18</sup>W. M. Tsang, A. L. Stone, D. Otten, Z. N. Aldworth, T. L. Daniel, J. G. Hildebrand, R. B. Levine, and J. Voldman, *J. Neurosci. Methods* **204**, 355 (2012).
- <sup>19</sup>W. Lu, L. Qu, K. Henry, and L. Dai, *J. Power Sources* **189** (2), 1270 (2009).
- <sup>20</sup>X. F. Wei and W. M. Grill, *J. Neural Eng.* **6**, 046008 (2009).